Vietnam Journal of Catalysis and Adsorption
Tạp chí xúc tác và hấp phụ Việt Nam

https://chemeng.hust.edu.vn/jca/

Synthesis of molybdenum disulfide for the hydrogen evolution reaction electrocatalysts activity by electrochemical method

Mai Thi Thanh Thuy*, Nguyen Thi Van Anh, Mai Thi Xuan, Phan Thi Binh

Institute of Chemisty, Vietnam Academic of Science and Technology, 18 Hoang Quoc Viet, Cau Giay, Hanoi
Email: thuyttmai1980@gmail.com

ARTICLE INFO

Received: 18/9/2021
Accepted: 10/12/2021
Published: 20/12/2021

Keywords:

Thiomolybdates solution, Electrodeposition, HER, Molybdenum disulfide.

ABSTRACT

This research aims to synthesize MoS_2 thin film for the hydrogen evolution reaction (HER) by the electrochemical way. We investigated various electrochemical conditions, including the pH of electrolyte, the applied current density, and electrolysis time to find optimal synthesis mode. The obtained samples were characterized by scanning electron microscopy (SEM) images and X-ray diffraction (XRD) patterns to determine the morphology and crystal structure. The polarization curve confirmed the HER activity of MoS_2 thin film. The results indicated that the synthesized MoS_2 film had a perfect catalytic activity, as shown by the overpotential value at 10 mA/cm^2 and Tafel slope reached 144 mV and 56.2 mV/dec, respectively.

Introduction

Hydrogen, a clean energy carrier, is the potential fuel of the future because the only byproduct after burning hydrogen is water vapor without greenhouse gas emissions or any pollutants. Photoelectrochemical (PEC) water splitting using sunlight to dissociate water molecules into hydrogen and oxygen through PEC cells (also known as "artificial leaf") is one of the most promising methods to produce hydrogen. PEC cell includes a p-type semiconductor photoelectrode as a cathode electrode and an n-type semiconductor photoelectrode as an anode electrode [1].

Among the p-type semiconductors to make photocathode of PEC cells, Molybdenum disulfide (MoS_2) is potential material, which has attracted the attention of scientists in recent years because of its novel electronic, optical, high reliability, low cost, and non-toxic [2-4]. MoS_2 has a sandwich-like layer structure, in which the layer of molybdenum atoms disulfide lies between two layers of sulfur atoms. Each monolayer of the S-Mo-S atoms is linked by strong covalent bonds, and between the monolayers in the crystal structure are relatively weakly bound together by the Van der Waals bond. There are three structural forms of MoS_2, including 1*T*- (*Trigonal*), 2*H*- (*Hexagonal*), and 3*R*-MoS_2 (*Rhombohedral*). The 2H phase exists naturally in bulk MoS_2, with lattice parameters a=b=3.15 Å, and c=12.3 Å is a semiconductor with a bandgap of 1.29 eV for bulk and 1.8 eV for monolayer or several layers of MoS_2. While 1T phase, not found in nature, can conduct electricity like a metal [5].

The previous reports showed that the catalytic activity of MoS_2 was significantly increased, higher than that of metal phosphides [6-8], and phosphor sulfide [9]. According to experimental studies [10] and theoretical calculations [10], the active centers at the edge in the

https://doi.org/10.51316/jca.2022.037

crystal structure of MoS_2 keep an important role in the catalytic reaction. Even the free energy of the hydrogen adsorption process on active centers at the edge of MoS_2 results close to Pt [11]. Thus, MoS_2 is a promising material to replace Pt for the HER catalytic activities. MoS_2 can be synthesized by different methods such as thermal decomposition [12], hydrothermal [13,14], chemical vapor phase deposition [15,16], electrochemistry [17,18].

In this study, MoS_2 film was synthesized by electrochemical deposition with thiomolybdate solution as the electrolyte. The paper gave the optimal mode for the electrolytes and MoS_2 film synthesis process, including pH of electrolyte, electrolysis time and current density. The MoS_2 film was studied morphology, crystal structure, catalytic activity.

Experimental

Chemical and material

Hexaammonium heptamolybdate tetrahydrate ($(NH_4)_6Mo_7O_{24}.4H_2O$), sodium sulfide nonahydrate ($Na_2S.9H_2O$), ammonium chloride (NH_4Cl), ammonia solution (NH_3), sulfuric acid (H_2SO_4, 95-98%), Ti foil (99.7%) were purchased from China.

Synthesis of thiomolybdate solution

Thiomolybdates solution was synthesized by chemical method following the steps. The first, $(NH_4)_6Mo_7O_{24}.4H_2O$ and $Na_2S.9H_2O$ were dissolved in a buffer solution with mass ratio $(NH_4)_6Mo_7O_{24}.4H_2O$: $Na_2S.9H_2O$ = 1:6. Then the mixed solution was heated at 90°C for 2 hours under continuous stirring. After that, the obtained thiomolybdates solution was used to synthesize the MoS_2 film.

Synthesis of electrocatalysis MoS_2

Ti electrode with size (0.8 cm x 0.8 cm x 0.1 mm) was soaked in the degreasing solution and cleaned with deionized water. Finally, it was dried at room temperature.

The MoS_2 film was prepared on the cleaned Ti substrate by a galvanic technique, using a three-electrode cell with reference electrode (calomel), counter electrode (Platinum), and work electrode (Ti foil) in the above synthesized electrolyte solution. The obtained electrode was washed gently with alcohol and acetone to remove the residue substance on the electrode surface. Then the electrode after the above progress was annealed at 400 °C in 1 hour under N_2 gas condition

Characterization of materials

The morphology of samples was determined by SEM images carried out on the equipment FE-SEM Hitachi S-4800 (Japan). XRD diffraction pattern, used to recognize the crystal structure, was measured by D8 ADVANCE of Bruker (Germany) with the 2Θ range from 10° to 70°. The catalytic properties of MoS_2 film samples were measured by polarization curve at the scanning rate of 5 mV/s in the 0.5 M H_2SO_4 on the IM6 equipment (Germany) with a reference electrode (calomel), counter electrode (Platinum).

Results and discussion

Electrolyte

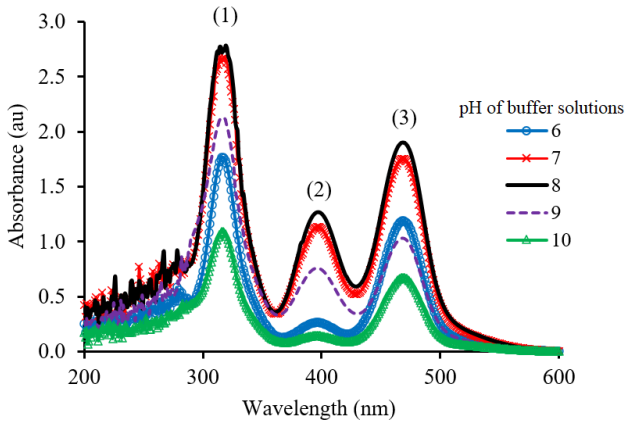

Figure 1: The UV-vis spectra of prepared thiomolybdate solutions with different pH buffer solutions.

Table 1: Peak positions of thiomolybdate solutions prepared from different pH

pH	UV-Vis					
	Peak 1 (nm)	Absor-bance (au)	Peak 2 (nm)	Absor-bance (au)	Peak 3 (nm)	Absor-bance (au)
6	317	1.767	396	0.266	469	1.190
7	318	2.677	397	1.133	469	1.756
8	319	2.786	397	1.270	468	1.904
9	317	2.133	396	0.759	468	1.032
10	317	1.092	396	0.145	469	0.675

https://doi.org/10.51316/jca.2022.037

Thiomolybdates solutions were prepared in the buffer solutions with a pH range changing from 6-10. Different pH of the buffer solutions leads to not only the different concentrations of thiomolybdate but also the change in the color of the obtained solutions that can be determined by UV-Vis Spectroscopy. The UV-vis spectra given in figure 1 show three peaks at the wavelength of around 317 nm (peak 1), 396 nm (peak 2), and 468 nm (peak 3) that reflect the $(MoO_2S_2)^{2-}$, $(MoOS_3)^{2-}$ and $(MoS_4)^{2-}$ ion features, respectively. This result is similar to previous work [19], and all the ions could produce molybdenum sulfide film by electrochemical method.

The intensity of the peak at 469 nm (peak 3) corresponding to $(MoS_4)^{2-}$ ion increased from 1.190 to 1.904 (a.u) with rising pH of the buffer solutions from 6 to 8. However, it then decreased to 0.675 at pH 10. This can be explained as follows. Firstly, in the low pH environment (pH 6), part of $(NH_4)_6Mo_7O_{24}.4H_2O$ decomposed easily to MoO_3 according to reaction (1) [20]. Secondly, the presence of NH_4^+ ion in the higher pH environment (pH 7, 8) will make $(NH_4)_6Mo_7O_{24}$ convert into diammonium molybdate $(NH_4)_2MoO_4$ according to equation (2). This substance will participate in the reaction to produce ammonium thiomolybdate according to reaction equation (3) [21]. But, a further increase in the pH of the medium (pH 9,10) limits reaction (3). Thus, the most suitable pH of the buffer solution for the synthesis of thiomolybdate from heptamolybdate was 8.

$$(NH_4)_6(Mo_7O_{24}) \rightarrow 7MoO_3 + 3H_2O + 6NH_3 \quad (1)$$

$$(NH_4)_6(Mo_7O_{24}) + 8NH_4^+ + 8OH^- \rightarrow 7(NH_4)_2(MoO_4) + 4H_2O \quad (2)$$

$$(MoO_4)^{2-} + 6S^{2-} + 8H_2O \rightarrow (MoS_4)^{2-} + 12OH^- + 2H_2S \quad (3)$$

Characterization of MoS_2

XRD

Figure 2 shows the X-ray patterns of obtained films before and after annealing. Similarly, to the published reports [19,21], the obtained film after electrodeposition with ammonium thiomolybdate as the electrolyte solution had an amorphous structure due to the fact that the product after the electrolysis process was MoS_x generated from the reaction (4).

$$(MoS_4)^{2-} + (10-2x)H^+ + 2e^- \rightarrow MoS_x + (4-x)H_2S\uparrow + H_2\uparrow \quad (4)$$

$$MoS_x \rightarrow MoS_2 + (x-2)\,S \quad (5)$$

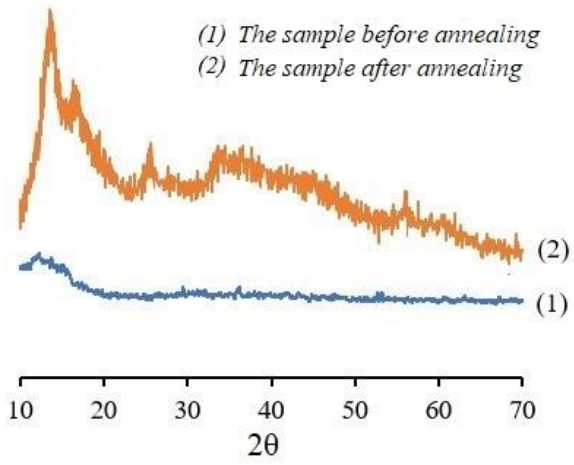

Figure 2: XRD patterns of MoS_2

After annealing at 400 °C for 1 h under N_2 gas condition, MoS_x decomposed into MoS_2 following the reaction (5). This is demonstrated by the XRD patterns of the samples before and after calcination (fig. 2). The XRD pattern of the sample before annealing (line 1) had no peak because of MoS_x in amorphous form. However, there is one major peak at 2 theta value of 13.8 and three small peaks at 2 theta values (25.3, 33.9, 56.4) on line 2. These obtained diffraction peaks of the sample after annealing were suitable with the standard data JCPDS (No. 37-1492), which evidenced the crystal structure of 2H-MoS_2 [22-24]. In brief, MoS_2 was successfully synthesized by combining the electrochemical with the thermal method.

SEM

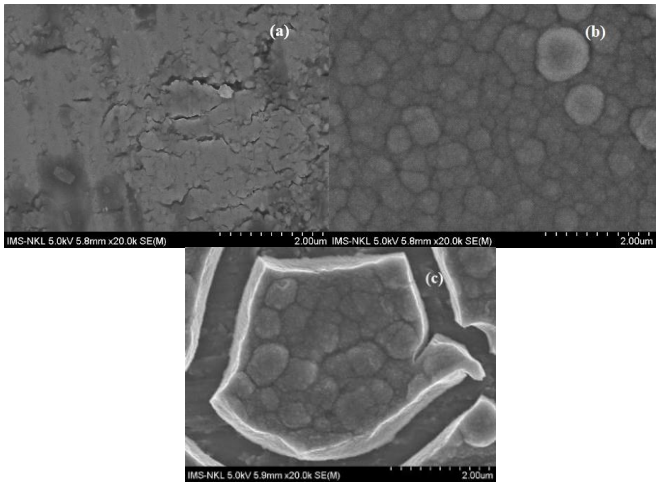

Figure 3: The SEM images of Ti substrate (a), MoS_2 film (b), MoS_2 film after HER activity (c)

The morphology of MoS_2 film before and after HER activity on the Ti substrate and Ti substrate was seen

https://doi.org/10.51316/jca.2022.037

clearly in fig 3. The SEM image of Ti foil given in fig 3a indicates that its surface is uneven and has many small cracks. After depositing MoS_2 on the Ti substrate, the electrode surface contains many small particles packed tightly together to form the film (see fig 3b). Fig 3c shows the surface of MoS_2 film after HER activity. It is obvious that the thin film is broken, and large cracks appear to reveal Ti background.

Effect of the electrolysis time on HER activity

The HER activity of samples synthesized at a constant current density of 2 mA/cm^2 and the electrolysis time varying from 15 to 75 mins was investigated by the polarization method. The total charge Q in the electrolysis process was calculated according to Faraday's law (6) (the Q value shown in table 2)

$$Q = I.t = i.S.t \quad (6)$$

where I is current (in A), t is time (in s), Q is quantity of electricity (in C), i is current density (in A/cm^2), S is area of electrode (in cm^2).

Figure 4 and Table 2 show that the obtained samples with different electrolysis times or the increase of total charge lead to variable HER activities. Firstly, it can be clearly seen on the polarization curves in fig 4a that all the MoS_2 thin films had much higher catalyst activity than the Ti substrate sample. The Tafel slope value of the Ti sheet was quite high at 201.8 mV/dec, while that values of MoS_2 samples were lower in the range of 74.6 to 83 mV/dec. Secondly, the overpotential value at 10 mA/cm^2 of samples displayed a significant reduction from 221 mV to 166 mV with the growth of electrolysis time from 15 mins to 60 mins before slight rising to 171 mV/dec at electrolysis time of 75 mins. Similarly, the lowest corresponding Tafel slope of the sample of 74.6 mV/dec was achieved for the electrolysis time of 60 mins. Furthermore, the current densities at the overpotential of 150, 200, and 250 mV of this sample had the highest values that exhibited the highest catalyst activity for hydrogen evolution reaction. To sum up, these results indicated that the sample electrolyzed with i= 2 mA/cm^2 for 60 mins (equivalent to the total charge Q= It=4.608 C) had the best catalyst activity for hydrogen evolution reaction.

It can be explained that the samples MoS_2 with different electrolysis times will vary the thickness of the film, which affects on properties of MoS_2 [5,25]. According to a previous report, the quantum yield of MoS_2 dropped with increasing thickness of the thin film, which reduced the threshold of generating electronic-hold pairs [25]. This was the reason why the catalyst activity of MoS_2 film decreased when the electrolysis time changed from 60 mins to 75 mins.

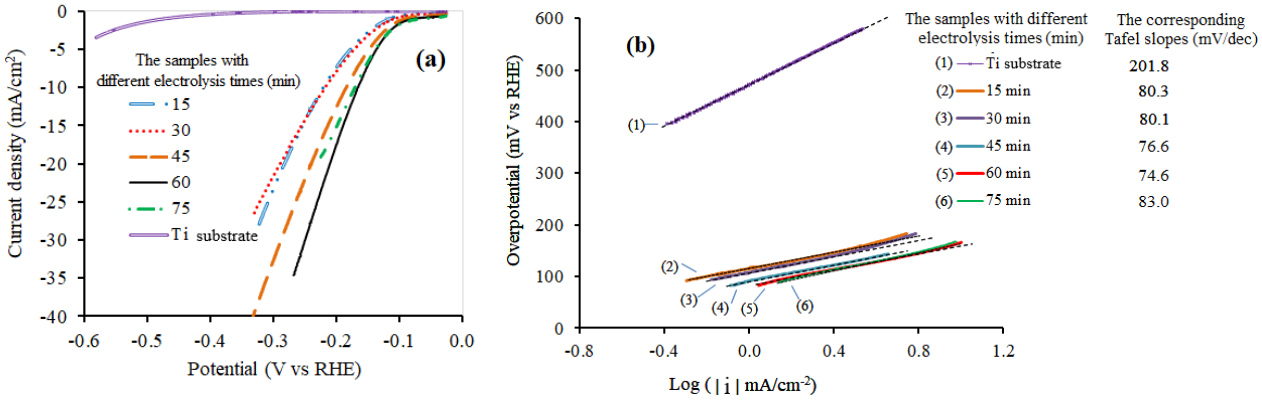

Figure 4: Polarization curves for HER of samples with different electrolysis times in 0.5M H_2SO_4 (a), Corresponding Tafel slopes (b)

Table 2: Comparison of HER electrocatalytic activity of samples with different electrolysis times

Electrolysis time (min)	The electric charge (C)	i (mA/cm^2) U = 150 mV	i (mA/cm^2) U = 200 mV	i (mA/cm^2) U = 250 mV	Overpotential (mVvs.RHE) at i=10(mA/cm^2)	Tafel slop (mV/dec)
15	1.152	2.74	7.33	14.30	221	80.3
30	2.304	3.17	7.92	14.20	218	80.1
45	3.456	5.21	12.60	21.90	184	76.6
60	**4.608**	**7.08**	**17.50**	**30.00**	**166**	**74.6**
75	5.760	6.63	15.20	-	171	83.0

https://doi.org/10.51316/jca.2022.037

Effect of the current density on HER activity

From the above result, the total charge Q = 4.608 C was selected to investigate the influence of current density on the catalytic activity of MoS_2 film.

Figure 5 and table 3 illustrate the influence of current density on the catalytic activity of MoS_2. It's obvious that after the dramatic drop from 75 to 56 in the range of current densities between 1.5 and 2.5 mA/cm^2, the corresponding Tafel slopes of the MoS_2 increased slightly to 60.6 mV/dec. Similarly, the lowest point of the overpotential value at 10 mA/cm^2 reached 144 mV at current density i= 2.5 mA/cm^2. In general, the sample at current density i =2.5 mA/cm^2 displayed the highest HER activity; moreover, the corresponding Tafel slope and overpotential value were smaller than the results of many previous public papers such as MO_3-MoS_2 hybrid nanospheres (200 mV and 74 mV/dec) [26], amorphous MoS_x film (211 mV and 55 mV/dec) [19], N doped MoS_2 (232 mV and 127 mV/dec) [30], NiS@MoS_2 core-shell microspheres (208 mV and 62.4 mV/dec) [31], MoS_x/V_2O_3 (145 mV and 45 mV/dec) [34] (it can be observed more information on table 3).

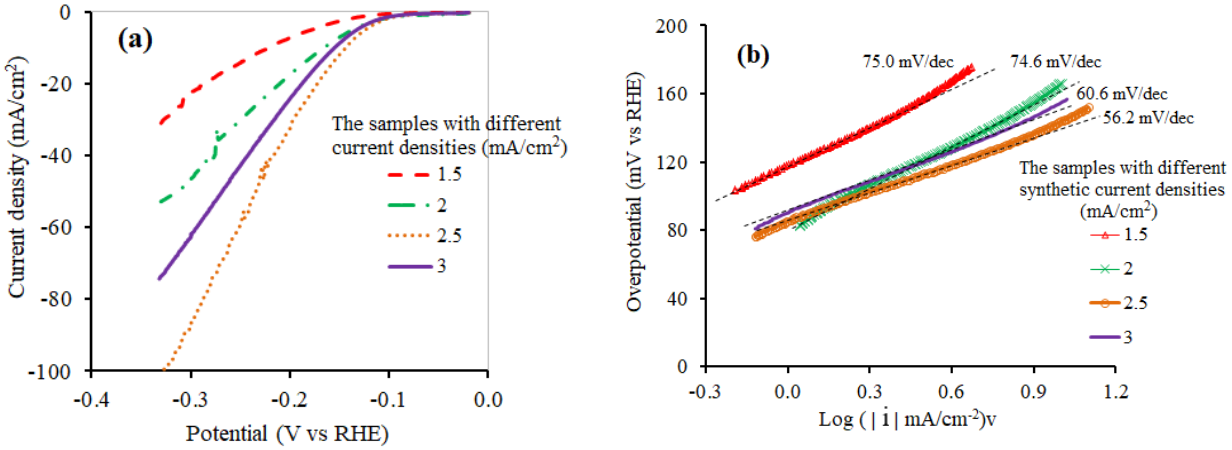

Figure 5: Polarization curves for HER of samples with different current densities in 0.5M H_2SO_4 (a), Corresponding Tafel slopes (b)

Table 3: Comparison of HER electrocatalytic activity of MoS_2 films with different current densities and other work values.

Ref.	Catalysts	Electrolyte	Overpotential at 10(mA/cm^2) (mV)	Tafel slop (mV/dec)
This work	Sample-1.5mA/cm^2	0.5M H_2SO_4	222	75
This work	Sample-2.0mA/cm^2	0.5M H_2SO_4	166	74.6
This work	**Sample-2.5mA/cm^2**	0.5M H_2SO_4	**144**	**56.2**
This work	Sample-3.0mA/cm^2	0.5M H_2SO_4	155	60.6
[19]	Amorphous MoSx film	0.5M H_2SO_4	211	55
[26]	NiO/MoS_2	1M KOH	158	109
[27]	MO_3-MoS_2 hybrid nanospheres	0.5M H_2SO_4	200	74
[28]	MoS_2/graphite	0.5M H_2SO_4	183	77.6
[29]	MoS_2@ CoS_2	1 M KOH	82	70
		1M PBS (*)	145	94
[30]	N doped amorphous MoS_x	0.5M H_2SO_4	143	57
	N doped MoS_2	0.5M H_2SO_4	232	127
[31]	MoS_2/graphene/carbonized melamine foam composite	1 M KOH	163	76
[32]	NiS@MoS_2 core-shell microspheres	0.5M H_2SO_4	208	62.4
		1M KOH	146	79.8
[33]	Peanut shells/MoS_2	0.5M H_2SO_4	154	71
[34]	MoS_x/V_2O_3	0.5M H_2SO_4	146	45

(*) *PBS: phosphate-buffered saline*

https://doi.org/10.51316/jca.2022.037

Conclusion

In summary, MoS_2 thin film using for HER electrocatalysts activity was synthesized successfully by the electrochemical deposition with thiomolybdate solution as the electrolyte. Ammonium thiomolybdate solution was prepared simply from ammonium heptamolybdate tetrahydrate with suitable pH of the buffer solution (pH=8). The MoS_2 thin film synthesized at the optimal condition of current density i = 2.5 mA/cm^2 and electrolysis time t = 60 mins had the highest HER activity efficiency. The overpotential value at 10 mA/cm^2 and the corresponding Tafel slopes of this sample were lower than other public papers and reached 144 mV and 56.2 mV/dec, respectively.

Acknowledgments

This research is funded by Institute of Chemistry under grant number VHH.2021.17

References

1. T.Bak, J. Nowotny ,M. Rekas, C.C. Sorrell, Inter. J. of Hydrogen Energy 27 (2002) 991 – 1022. https://doi.org/10.1016/S0360-3199(02)00022-8.
2. Qi Ding, Bo Song, Ping Xu, Song Jin, Chem, 1 (2016) 699-726. https://doi.org/10.1016/j.chempr.2016.10.007
3. Uttam Gupta, C.N.R.Rao, Nano energy, 41 (2017) 49-65. https://doi.org/10.1016/j.nanoen.2017.08.021
4. Effat Sitara , Habib Nasir , Asad Mumtaz , Muhammad Fahad Ehsan , Manzar Sohail, Sadia Iram, Syeda Aqsa Batool Bukhari, Nanomaterials, 10 (2020) 2341. https://doi.org/10.3390/nano10122341
5. F. Mak, C. Lee, J. Hone, J. Shan, T.F. Heinz, Phys. Rev. Lett, 105 (2010) 136805–136808. https://10.1103/PhysRevLett.105.136805
6. Vesborg P.C.K, Seger B, And Chorkendorff I, J. Phys. Chem. Lett., 6 (2015) 951–957. https://doi.org/10.1021/acs.jpclett.5b00306
7. Popczun E.J, Mckone J.R, Read, C.G, Biacchi A.J, Wiltrout A.M, Lewis N.S, And Schaak R.E, J. Am. Chem. Soc, 135 (2013) 9267–9270. https://doi.org/10.1021/ja403440e
8. Callejas J.F, Read C.G, Roske C.W, Lewis N.S, And Schaak R.E, 28 (2016) 6027–6044. https://doi.org/10.1021/acs.chemmater.6b02148
9. Caban-Acevedo M, Stone M.L, Schmidt J.R, Thomas J.G, Ding Q, Chang H.C, Tsai M.L, He J.H, Jin S, Nat. Mater,14 (2015) 1245–1251. https://doi.org/10.1038/nmat4410
10. Jaramillo T.F, Jorgensen K.P, Bonde J, Nielsen J.H, Horch S, And Chorkendorff I, Science, 317 (2007) 100-102. https://10.1126/science.1141483.
11. Hinnemann B, Moses P.G, Bonde J, Jorgensen K.P, Nielsen J.H, Horch S, Chorkendorff I, Norskov J.K, J. Am. Chem. Soc, 127 (2015) 5308–5309. https://doi.org/10.1021/ja0504690
12. Zhenhua Lou, Di Wu, Kun Bu, Tingting Xu, Zhifeng Shi, Junmin Xu, Yongtao Tian, Xinjian Li, Journal of alloys and compounds, 726 (2017) 632- 637. https://doi.org/10.1016/j.jallcom.2017.07.338
13. Nahid Chaudhary, Manika Khanuja, Abid, S.S. Islam, Sensors and actuators A, 277 (2018) 190–198. https://doi.org/10.1016/j.sna.2018.05.008
14. Lijuan Ye, Haiyan Xu, , Shijian Chen, Material reseach bulletin, 55 (2014) 221-228. https://doi.org/10.1016/j.materresbull.2014.04.025
15. Shuang Liu, Changbin Nie, Dahua Zhou, Jun Shen, Shuanglong Feng, Physica E: low-dimensional systems and nanostructures, 117 (2020) 113592. https://doi.org/10.1016/j.physe.2019.113592
16. Jie Zhang, Tianyu Liu, Liangjie Fu, Gonglan Ye, Chemical physics letters, 781 (2021) 138972. https://doi.org/10.1016/j.cplett.2021.138972
17. Akif Shikhan Aliyev, Mahmoud Elrouby, Samira Fikret Cafarova, Materials science in semiconductor processing, 32, (2015) 31–39. https://doi.org/10.1016/j.mssp.2015.01.006
18. Megha Shrivastava, Reeta Kumari, Mohammad Ramzan Parra, Padmini Pandey, Hafsa Siddiqui, Fozia Z. Haque, Optical material, 73 (2017) 763-771. https://10.1016/j.optmat.2017.09.029
19. Lina Zhang, Liangliu Wu, Jing Li And Jinglei Lei, BMC chemistry,13:88 (2019) https://doi.org/10.1186/s13065-019-0600-0
20. Tzu Hsuan Chiang, Hung Che Yeh, Materials, 6 (2013) 4609-4625. https://10.3390/ma6104609
21. S.K. Ghosha, T. Bera, O. Karacasua, A. Swarnakar, J.G. Buijnsters, J.P. Celis, Electrochimica Acta, 56 (2011) 2433-2442. https://10.1016/j.electacta.2010.10.065
22. Pravas Kumar Panigrahi, Amita Pathak, Journal of Nanoparticles, 2013, 671214. https://doi.org/10.1155/2013/671214
23. Tuhin Subhra Sahu, Sagar Mitra , Scientific Reports, 5 (2015) 12571 .

https://doi.org/10.1038/srep12571

24. Xia Li, Bo Wang, Xia Shu, Dongmei Wang, Guangqing Xu, Xinyi Zhang, Jun Lv, Yucheng Wu, RSC Advances, 9 (2019) 15900–15909. https://doi.org/10.1039/C8RA09806A
25. Xin-Wei Yang, Xiao-Ping Wang, Li-Jun Wang, Diamond and Related Materials, 114 (2021) 108331. https://doi.org/10.1016/j.diamond.2021.108331
26. Kai Xia, Meiyu Cong, Fanfan Xu, Xin Ding, and Xiaodong Zhang, Nanomaterials, 10 (2020) 1547. https://doi.org/10.3390/nano10081547
27. Xuebin Houa, Alfred Mensaha, Min Zhaoa, Yibing Caia, Qufu Wei, Applied surface science, 529 (2020) 147115. https:// 10.1016/j.apsusc.2020.147115
28. Chia Chin cheng, Ang Yu Lu, Chien Chih Tseng, Xiulin Yang, Mohamed Nejib Hedhili, Min Cheng Chen, Kung Hwa Wei, Lain Jong Li, Nano energy, 30 (2016) 846-852. https://doi.org/10.1016/j.nanoen.2016.09.010
29. Shasha Li, Suchada Sirisomboonchai, Xiaowei An, Xuli Ma, Peng Li, Lixia Ling, Xiaogang Hao, Abuliti Abudula, Guoqing Guan, Nanoscale, 12 (2020) 6810-6820. https://doi.org/10.1039/D0NR00008F
30. Ruimin Ding, Mengchao Wang, Xianfen Wang, Huixiang Wang, Liancheng Wang, Yuewen Mu, Baoliang Lv , Nanoscale, 11 (2019) 11217-11226. https://doi.org/10.1039/C9NR02717C
31. Wen Li, Jun-wei Chen, Zong-liang Xiao, Jing-bo Xing, Chen Yang, Xiao-peng Qi, New Carbon Materials, 35 (2020) 540-546. https://10.1016/S1872-5805(20)60507-8
32. Zhiwen Chen, Xiao Liu, Peijun Xin, Haitao Wang, Ye Wu, Chunyan Gao, Qingquan He, Yong Jiang, Zhangjun Hu, Shoushuang Huang, Journal of Alloys and Compounds, 853 (2021) 157352. https://doi.org/10.1016/j.jallcom.2020.157352
33. Huan Chen, Haichao Jiang, Xuepu Cao, Yantao Zhang, Xiangjing Zhang, Shanlin Qiao, Materials Chemistry and Physics, 252 (2020) 123244. https://doi.org/10.1016/j.matchemphys.2020.123244
34. Mingwei Hu, Jin Huang, Qizhong Li, Rong Tu, Song Zhang, Meijun Yang, Haiwen Li, Takashi Goto, Lianmeng Zhang, Journal of Alloys and Compounds, 827 (2020) 154262. https://doi.org/10.1016/j.jallcom.2020.154262